Journal of
Manufacturing and Materials Processing

MDPI

Article

Manufacturing of High Conductivity, High Strength Pure Copper with Ultrafine Grain Structure

Leila Ladani [1,*], Jafar Razmi [2] and Terry C. Lowe [3]

[1] School of Engineering of Matter, Transport and Energy, Arizona State University, Tempe, AZ 85281, USA
[2] School of Sustainable Engineering and Build Environment, Arizona State University, Tempe, AZ 85281, USA; jafar.razmi@asu.edu
[3] Department of Metallurgical and Materials Engineering, Colorado School of Mines, Golden, CO 80401, USA; lowe@mines.edu
* Correspondence: ladani@asu.edu

Abstract: Applications of Copper (Cu) range from small scale applications such as microelectronics interconnects to very large high-powered applications such as railguns. In all these applications, Cu conductivity and ampacity play vital roles. In some applications such as railguns, where Cu also plays a structural role, not only is high conductivity needed, but high strength, high ductility, and high wear resistance are also critical. Current technologies have achieved their full potential for producing better materials. New approaches and technologies are needed to develop superior properties. This research examines a new fabrication approach that is expected to produce Cu with superior mechanical strength, enhanced wear resistance, and increased electrical conductivity. Materials with refined grain structures were obtained by breaking down the coarse-grained Cu particles via cryogenic ball milling, followed by the consolidation of powders using cold isostatic pressing (CIP) and subsequent Continuous Equal Channel Angular Pressing (C-ECAP). The mixture of fine and ultrafine grains, with sizes between 200 nm to 2.5 µm and an average of 500 nm, was formed after ball milling at cryogenic temperatures. Further processing via C-ECAP produced nanostructured Cu with average grain sizes below 50 nm and excellent homogenous equiaxed grain shapes and random orientations. The hardness and tensile strength of the final Cu were approximately 158% and 95% higher than the traditional coarse-grained Cu bar, respectively. This material also displayed a good electrical conductivity rate of 74% International Annealed Copper Standard (IACS), which is comparable to the current Cu materials used in railgun applications.

Keywords: Copper; high conductivity; high strength; ultrafine grains

Citation: Ladani, L.; Razmi, J.; Lowe, T.C. Manufacturing of High Conductivity, High Strength Pure Copper with Ultrafine Grain Structure. *J. Manuf. Mater. Process.* **2023**, *7*, 137. https://doi.org/10.3390/jmmp7040137

Academic Editor: Steven Y. Liang

Received: 28 June 2023
Revised: 25 July 2023
Accepted: 26 July 2023
Published: 30 July 2023

Copyright: © 2023 by the authors. Licensee MDPI, Basel, Switzerland. This article is an open access article distributed under the terms and conditions of the Creative Commons Attribution (CC BY) license (https://creativecommons.org/licenses/by/4.0/).

1. Introduction

Increasing strength in metals can typically occur through multiple mechanisms, including introducing foreign elements through alloying and increasing the density of planar and line defects such as grain boundaries and dislocations through plastic deformation. Alloying can introduce foreign atoms in the lattice structure and inhibit the dislocation motion due to stress fields resulting from atomic misfit, which in turn increases the material's strength [1]. Grain size reduction is a mechanism that is described by the Hall–Petch [2,3] relationship. However, these methods usually result in a reduction of ductility, which is oftentimes a necessary quality for the materials. Introduction of the nanoscale grains gave rise to a different phenomenon that occurs at length scales lower than 20 nanometers, namely the inverse Hall–Petch effect [4]. However, achieving such a small grain size is, in most cases, impractical or very costly. Efforts have been reported in the literature to balance the strength and ductility of the metals by creating bi-modal grain size distributions. Bi-modal grain size alloys are made with a mixture of coarse grains and ultrafine grain or nanostructured metal. The coarse grain structure provides ductility, and the nanostructured

matrix provides strength. Extensive analysis has been conducted on Al-Mg alloys and all have shown promising results [5–9].

Accordingly, for Cu, strengthening has been achieved through alloying, solid solution strengthening, precipitation hardening, grain refinement, severe plastic deformation, and nano-twinning [10–17]. Alloying the Cu matrix with other materials such as Cr, Zr, Zn, Al, Nb, and Al_2O_3 has shown excellent performance with improved mechanical strength. Cu-Cr alloys with a very small amount of Cr are a common two-phase age hardening alloys with improved strength because of the dispersed phase [13,18,19]. Furthermore, increasing the Cr percentage can enhance the strength and hardness in Cu-Cr alloys [12]. This can be explained by the higher dislocation density and smaller grain size due to the pinning effect (dispersion of fine particles) of chromium on lattice structures [13]. As Cr has very low solubility in Cu, only about 1.28 wt% of Cr is soluble in Cu at around 1080 °C. Cr concentration above the solubility limit in the alloy does not change the strength and electrical conductivity [13].

Because metal alloying can be very difficult sometimes, grain refinement by severe plastic deformation is another viable technique to improve the material properties. Cryo-milling, Cold Isostatic Pressing (CIP), and Equal Channel Angular Pressing (ECAP) are a few techniques that have been used to reduce the grain size. Milling the material at cryogenic temperatures has been shown to be very effective in producing ultrafine grain and nanocrystalline Cu [20].

CIP involves compacting powders in an elastomer mold into a solid homogeneous mass. The creation of materials by CIP causes them to have uniform strength, better corrosion resistance, improved ductility, and high green strength [21]. In ECAP, a high amount of shear strain produces plastic deformation when it has undergone multiple passes through a special die. This high strain also causes the alloy to have submicron-level grain sizes. In this method, very high pressure is applied to deform the material as it passes through an intersection of two channels, causing deformation in the material. ECAP tends to improve the hardness and tensile and compressive strengths, as well as improve corrosion resistance. The mechanical properties especially tend to improve after multiple passes [22].

However, it is not only desirable to improve the mechanical properties for applications such as railguns, the electrical conductivity is also very important. Many of the processes that cause grain refinement typically reduce the electrical conductivity as well. In some cases where the twin boundary density was increased, specifically in ECAP processes, the electrical conductivity was shown to have been unaffected or slightly increased [23,24].

Although nanocrystalline materials show greatly improved strength, they are accompanied by low ductility [25]. Therefore, keeping a certain percent coarse grain (CG) in the matrix (as in a bimodal grain size alloy) can help increase the ductility at the cost of a small reduction in strength. In addition to nanostructured grains, twin boundaries inside grain interiors have a strengthening effect on the material [11].The nanocrystalline (NC) Cu alloy with high density twins possesses greater yield strength than NC-Cu and CG-Cu alloys [26,27]. Therefore, it is desirable to increase twin boundaries in Cu to enhance the strength and conductivity. A combination of material processing that can generate the bi-modal grain size Cu and increase the twin boundary density ensures high mechanical strength and good electrical conductivity [28,29].

In this study, Cu particles are cryo-milled initially to reduce the grain size to achieve a bi-modal grain size microstructure in powder particles. Nanoscale grains provide strength, while coarse grains provide ductility. Breaking down the powder particle to an Ultrafine Grain (UFG) level is conducted at cryogenic temperatures, which is necessary to avoid joining and reforming the microscale powder [25,26,30]. This process, along with cold isostatic pressing, has been used in the past to produce high strength materials. However, nanostructured and ultrafine grain materials are known to have high electrical resistivity due to the presence of the grain boundaries that scatter electrons. The addition of twin boundaries has been shown to improve strength without decreasing electrical conductivity. This could

be achieved through Equal Chanel Angular Pressing (ECAP), which is a very effective Severe Plastic Deformation (SPD) technique [31]. This method is known to refine grain size and improve the strength in materials [32,33]. Additionally, it has shown how electrical conductivity can be enhanced in the materials by generating twin boundaries [23,24]. Characterization including Electron Backscattered Diffraction (EBSD) analyses, hardness tests, mechanical tests, and electrical conductivity tests were conducted at the intermediate steps, as well as at the final steps, to monitor and determine the improvements of these properties quantitatively over traditional methods.

Although grain size reduction is a common method in enhancing the strength of the material, it is oftentimes associated with reduced ductility and increased electrical resistivity. The literature has shown that achieving better results in all three aspects is yet to be attained through conventional manufacturing processes [28,32,33]. The process proposed and applied here will result in increasing ductility through additional coarse grains, increasing the electrical conductivity through creation of nanotwin boundaries, and increasing strength by reducing grain size to the nano-scale. This approach shows promising results that could potentially be helpful to many different applications, including aerospace and naval applications.

2. Materials and Experimental Procedures

Spherical Cu powders with 99% purity, particle sizes of 45–105 µm, and chemical composition matching those shown in Table 1 were obtained from the Stanford Advanced Materials company located in Lake Forest, CA. Cryo-milling of Cu powders was conducted inside a grinding tank in a rotating slurry environment consisting of the Cu powders, stainless steel balls, and liquid nitrogen (LN_2). The stainless steel balls with sizes of 3.175 mm and 6.35 mm were used as the grinding media. A Model Hd-01 Attritor from the Union Process, Inc located in Akron, OH (Figure 1) was used for the cryo-milling. The temperatures were kept between −180 °C to −196 °C. The Attritor with 1.4×10^6 mm^3 grinding tank has an agitator shaft with several arms to create the required circulating motion. Several experiments were conducted to obtain optimum parameters, namely the media/powder weight ratio, grinding media size and ratio, and the attritor rpm. Experimental parameters and their levels are shown in Table 2. Rather than randomly running certain parameters at certain levels using traditional Design of Experiment approaches, we chose to run the experiments intelligently, deciding after each run what parameters to change at what levels to achieve the desired outcome. Temperatures were kept at cryogenic levels with the help of a continuous supply of liquid nitrogen. This helps to prevent oxidation, recovery, and recrystallization in the powder grain structures [34–36].

Table 1. Chemical composition of 99% pure Cu powders.

Component	Weight Percentage (wt%)
Pb	0.01
Bi	0.01
Sn	0.01
Ni	0.002
Fe	0.01
As	0.005
Zn	0.01
Sb	0.001
S	0.005
O	0.08
Cu	Balance

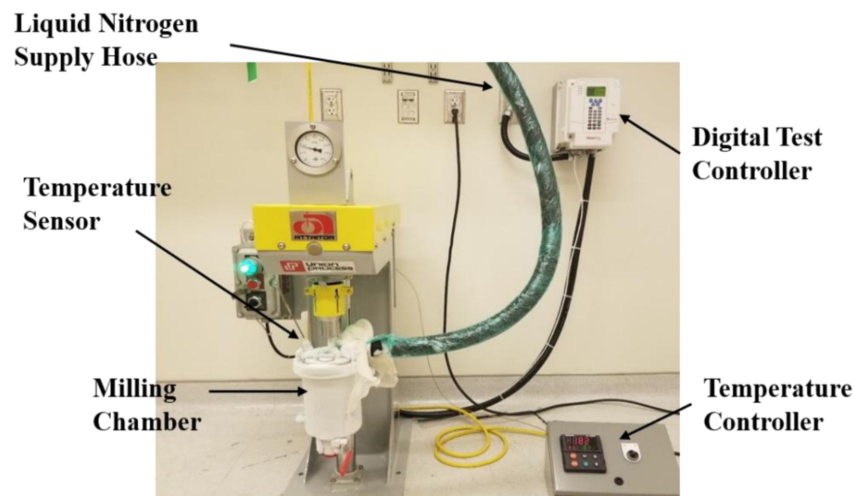

Figure 1. Model HD-01 Lab Attritor, cryogenic ball milling machine with various components.

Table 2. Summary of cryo-milling parameters.

	Ball Size (mm)	Ball: Powder (Weight Ratio)	Speed (rpm)	Time (Hours)	Results
Run 1	6.35	32:1	190	4	No significant change in particle size
Run 2	6.35	1.6:1	310	4	Particle size increased from 55 microns to 81 microns
Run 3	6.35	2:1	600	3	No significant changes observed
	6.35 replaced by 3.75			4	After 3 h of grinding with 1/4 balls, the balls were replaced with 1/8 balls and grinding continued for another 4 h. Resulted in Bi-modal particle size.
Run 4	3.75	2:1	600	7.5	Flattening of particles occurred
	3.175 replaced by 3.175 + 6.35 (1:1)			4	Further flattening of the particles and fracture into smaller pieces resulting in bi-modal particle sizes with a large difference in average particle size in two large and small modes

After each run, the particle size distributions of pure Cu were measured from the scanning electron microscope (SEM) images of them using ImageJ software. The SEM images were taken using a ZEISS FIB-SEM (Focused Ion Beam-SEM) instrument. The grain size distribution of as-received pure Cu and cryo-milled Cu were analyzed further using the OIM Analysis v8 software.

The cryo-milled powders with bi-modal grains comprised of UFG and Fine Grain (FG) sizes were then consolidated by cold isostatic pressing (CIP) using a Simac Monostatic Dry Bag Isostatic Press (362,000 kg) from Gasbarre Products, Inc, shown in Figure 2. Polyurethane molding bags along with steel top/bottom punches were used for the consolidation process. During CIP, the custom-made polyurethane molding bag filled with the selected alloy powders was placed in a pressure chamber filled with a liquid medium, and a high pressure was then applied uniformly from all sides for the consolidation to occur. Both cryo-milled and un-milled powders were consolidated using the CIP process. The process was conducted at ambient temperatures 150°F, 200°F, and 250°F. Low CIP

temperatures prevented the grain growth and recovery due to elevated temperatures [1]. Pressure levels of 138 MPa, 172 MPa, 207 MPa, 303 MPa for un-milled Cu and 207 MPa and 303 MPa for cryo-milled Cu were applied to find the optimum pressure levels. The dwell time used was 3 sec, which was followed by a flash decompress.

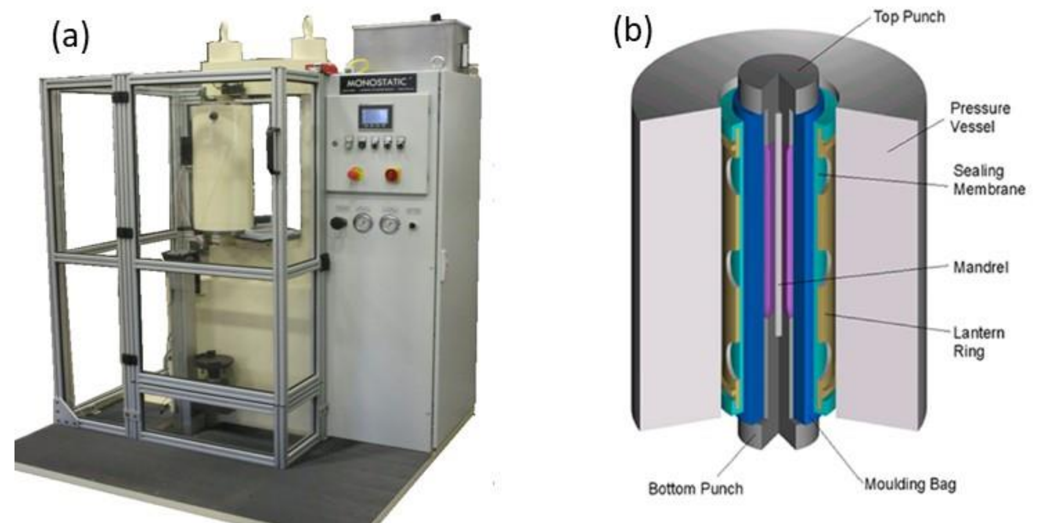

Figure 2. Simac Monostatic Dry Bag Isostatic Press (**a**) the actual machine, (**b**) drawing with various inner components.

CIPed samples were further investigated using 3-dimensional (3D) X-ray computed tomography (CT) scans. A ZEISS Xradia 520 instrument with a maximum voltage of 160 kV and power of 10 W was used for this purpose.

The CIP-consolidated sample was further processed using a Continuous Equal-Channel Angular Pressing (C-ECAP) machine. Initial trials were conducted at room temperature and 0.8 mm/s speed to validate processing without any lubricant because of the porous structure of the sample. To avoid sample breakage, the samples were inserted between two AA6201 aluminum billets, which provided high compressive forces to further compact the samples prior to entering the C-ECAP shear zone and minimize interaction with the tooling. The C-ECAP process was adjusted to use temperatures slightly above room temperature to avoid fracture. Prior to being fed into the heated C-ECAP Machine on each pass, samples were soaked in a tube furnace adjacent to the machine for 10 min at 125 °C. Samples were subject to a 6.3 mm/s feed rate and temperatures of 130–140 °C during C-ECAP. For all processing, the machine was set-up using the tooling with a 12 mm die channel and 120° shear die. Four passes of C-ECAP were applied to all samples.

Optical microscopy was conducted using an Olympus MX50 microscope equipped with a Sony DXC-970MD 3CCD Color Camera. The electron backscatter diffraction (EBSD) analysis was conducted using a ZEISS FIB-SEM instrument equipped with an EDAX® | AMETEK® EBSD detector. The crystallographic samples were prepared using a standard polishing process. The Cu powders were polished gradually to the finer silicon carbide (SiC) grit sizes. The final stages of the polishing were performed using 1 µm, 0.25 µm, and 0.1 µm diamond suspensions, respectively, and polishing cloth combinations. The polishing machine and materials were provided through Pace Technology. The samples were cleaned properly using a soap solution between the steps to prevent the carryover of coarser particles to the next level. Finally, the polished surfaces were further cleaned using acetone, methanol, and isopropyl alcohol (IPA), respectively, to remove any foreign particles.

The electrical conductivity of the fabricated Cu sample was evaluated by the Sigmascope SMP350 instrument. The calibration was done using a Cu standard. To assess the surface mechanical properties of the sample after C-ECAP, nanoindentation was done using an MTS nanoindenter XP with a Berkovich diamond tip. Initial calibration was done using

fused silica. A minimum of nine indents were made with 50 µm spacing between two indents to avoid any overlap of their plastic zones.

3. Results

3.1. Cryo-Milling of Powders

The process started with pure Cu with an average particle size of 55 µm and a range of 18–117 µm. A fair level of sphericity was observed in the initial particle size distribution. The pure powder was then cryo-milled under a different set of parameters, as outlined in Table 2. Cryo-milling is a mechanical attrition process conducted within a cryogenic environment that is used to strengthen the material and to decrease the size of the particles and the spacing inside a metallic alloy [37]. Previous studies showed that during ball milling, the coarse powder particles undergo continuous flattening, cold welding, and eventually fracturing into finer particles. The flattening and cold welding take place during the initial stages of milling when the powders are comparatively soft, but after a certain period of milling, the particles become work hardened due to steady state deformation and fracture into very fine particles with excellent grain refinement [34–42]. The milling duration required for the desired grain refinement of various Cu and aluminum alloys ranged between 4-12 h depending on the milling environment and parameter used.

The evolution of powder particles at different steps of cryo-milling are presented in Figures 3 and 4. For the first two runs listed in Table 2, where speeds of 190 and 310 rpm and a ball medial diameter of 1/4 in balls were used, no significant changes in particle sizes were observed. The sphericity of the powder particles seemed to have been preserved with no flattening of particles nor changes in particle sizes observed. To expedite the process accordingly, the speed was increased to 600 rpm and the amount of powder was increased to have a ball to powder ratio of 2:1. After 3 h of milling with a ball to powder ratio of 2:1, a speed of 600 rpm, and grinding media with the size of 6.35 mm, some changes to particle distribution were observed. Interestingly, at this stage a bi-modal powder size was observed, where both large particles mixed with a much smaller particle size distribution exist simultaneously. However, the smallest size of the particles was still larger than a few microns, as displayed in Figure 3a–e. To obtain better refinement, as part of the same experimental run, the 6.35 mm grinding media was replaced by finer 3.175 mm grinding balls. The smaller size media was expected to further reduce the particle sizes. After 3 h of milling the same powder with smaller-sized media, the same bi-modal size particles seemed to have been generated. However, this method resulted in more flattening of the particles with a larger difference in average size between the large and small particles, with the size of the small particle distribution still above a few microns. Large particles deformed to flat particles and the sphericity of the particles was lost. It appears that cold-welded, highly flattened particles were fragmented to very fine powder particles, as can be seen in Figure 3g,h. According to the literature findings, during the initial flattening and cold welding period of the milling process, the localization of deformation generates shear bands, and the dislocation density increases significantly [35,37]. After further milling, the annihilation and recombination of dislocations further create nanoscale sub-grain structures. These sub-grain structures then turned into randomly orientated high-angle grain boundaries [35,37].

In the next step of optimization runs, another combination of grinding media was used in order to examine their milling outcomes. Initially, only the 3.6 kg of finer grinding media (with 3.175 mm size) was used to test their capability to produce finer powder particles. The grinding outcomes with the finer grinding media alone did not meet the expectation, as evidenced in Figure 4a–c. There were no substantial changes in powder particle sizes after 3.5 h of milling, though flattening of the powder particles was observed after 7.5 h of milling. Therefore, to accelerate the milling process, the 3.6 kg of 3.175 mm media was replaced by a mixture (1.8 kg of 6.35 mm + 1.8 kg of 3.175 mm) of grinding media. The mixing of grinding media indeed accelerated the milling process, as evidenced in Figure 4d,e. Significant flattening and cold-welding were observed after another 2 h of

grinding with mixed media. Again, the fracturing of the powder particles to finer sizes was observed after 4 h of milling with this updated combination of parameters. The powder from this combination of parameters was selected to be used in the next step of the process, which is the Cold Isostatic Process.

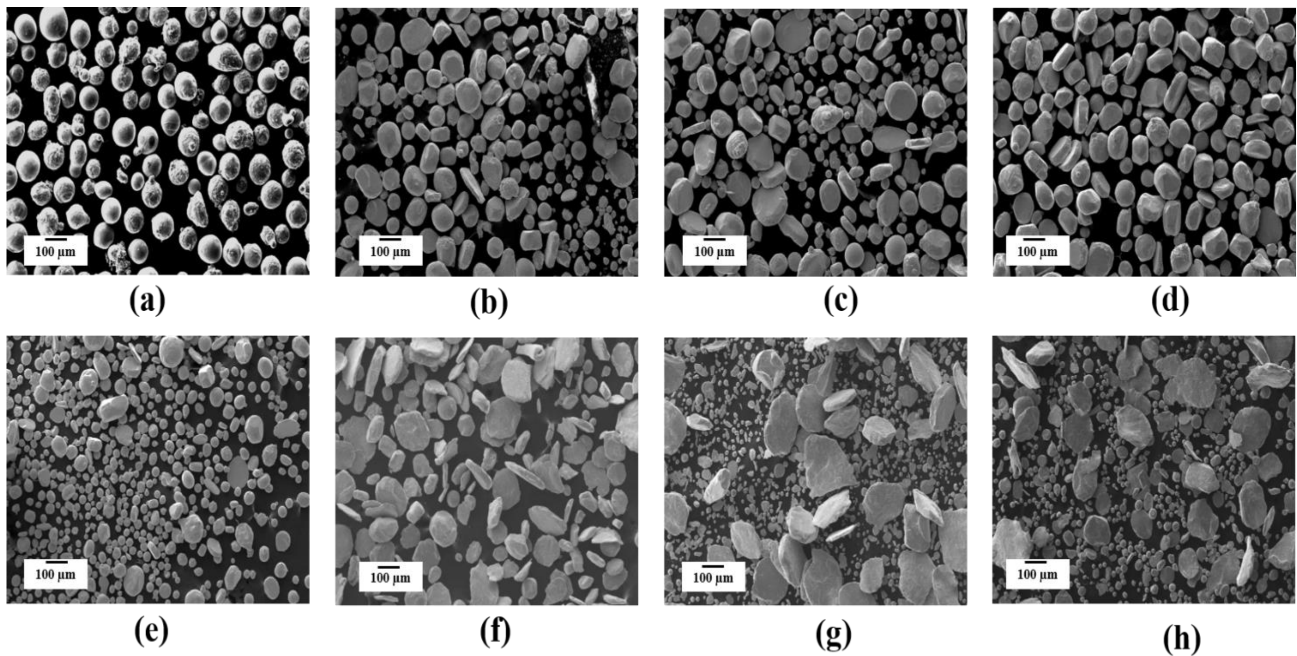

Figure 3. SEM images of (**a**) initial Cu powders, and after (**b**) 30 min, (**c**) 1 h, (**d**) 2 h, and (**e**) 3 h of cryo-milling with 6.35 mm grinding media, and after (**f**) 5 h, (**g**) 6 h, and (**h**) 7 h of cryo-milling with finer (3.175 mm) media.

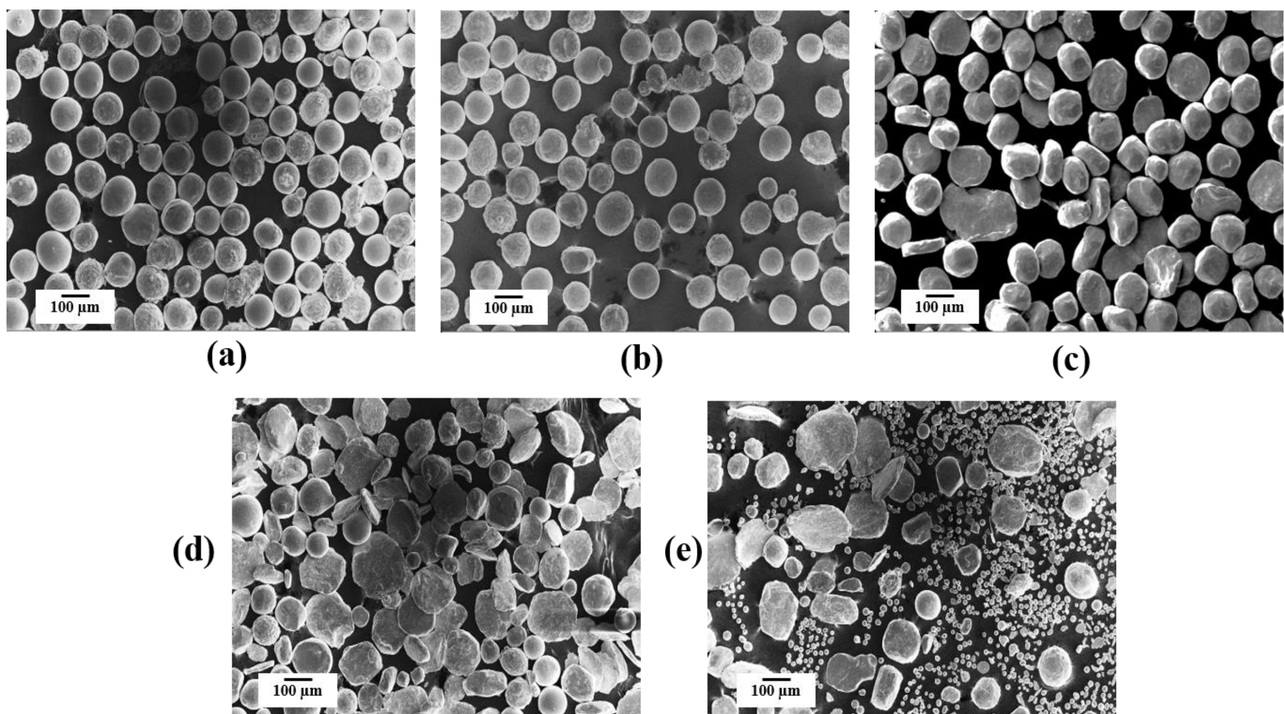

Figure 4. SEM images of (**a**) pure Cu after (**b**) 3.5 h and (**c**) 7.5 h of cryo-milling with finer grinding media (3.6 kg of 3.175 mm), and subsequent (**d**) 2 h and (**e**) 4 h of cryo-milling with mixed grinding media (1.8 kg of 6.35 mm + 1.8 kg of 3.175 mm).

3.2. Microstructural Analysis of Powder Particles

The literature has shown that during cryo-milling, the nanocrystalline structure is formed following several steps of grain refinement [11]. Initially, the localization of deformation turns into shear bands, increasing the dislocation density inside the coarse grain. Then, the nanoscale sub-grains are developed from the subsequent annihilation and recombination of those dislocations. Eventually, following the continuous milling, the sub-grain structure transforms into the high-angle grain boundaries with random orientations [38,39]. Because of the grain size refinement during cryo-milling, the grain boundary strengthening mechanism takes place, in which the high volumetric density of grain boundaries inhibits the dislocation movements and strengthens the materials. This is also known as the Hall–Petch effect [34]. According to the Hall–Petch grain boundary strengthening mechanism, the strength of the coarse-grained (CG, grain sizes > 3 µm) material increases as the grain sizes decreases towards fine-grained (FG, grain sizes ~1 µm to 3 µm), ultrafine-grained (UGF, grain sizes ~100 nm to 1000 nm), and nanostructured (NS, grain sizes, <100 nm) grained, respectively [34,36]. With sufficient cryo-milling of Cu powders, the grain sizes of the particles could be tailored according to the requirement of the user to obtain nanocrystalline or UFG bulk material with improved strength [39].

The as-received pure Cu powders exhibited dendrite microstructures comprised of coarse grains with sizes greater than 3 microns, as shown in Figure 5 (the top images). In contrast, the cryo-milled Cu powders displayed a deformed, randomly oriented equiaxed microstructure containing refined grains with sizes less than 3 microns, as shown in Figure 5 (the bottom images). The cryo-milling process significantly changed the initial low angular coarse grains to the high angular finer grains.

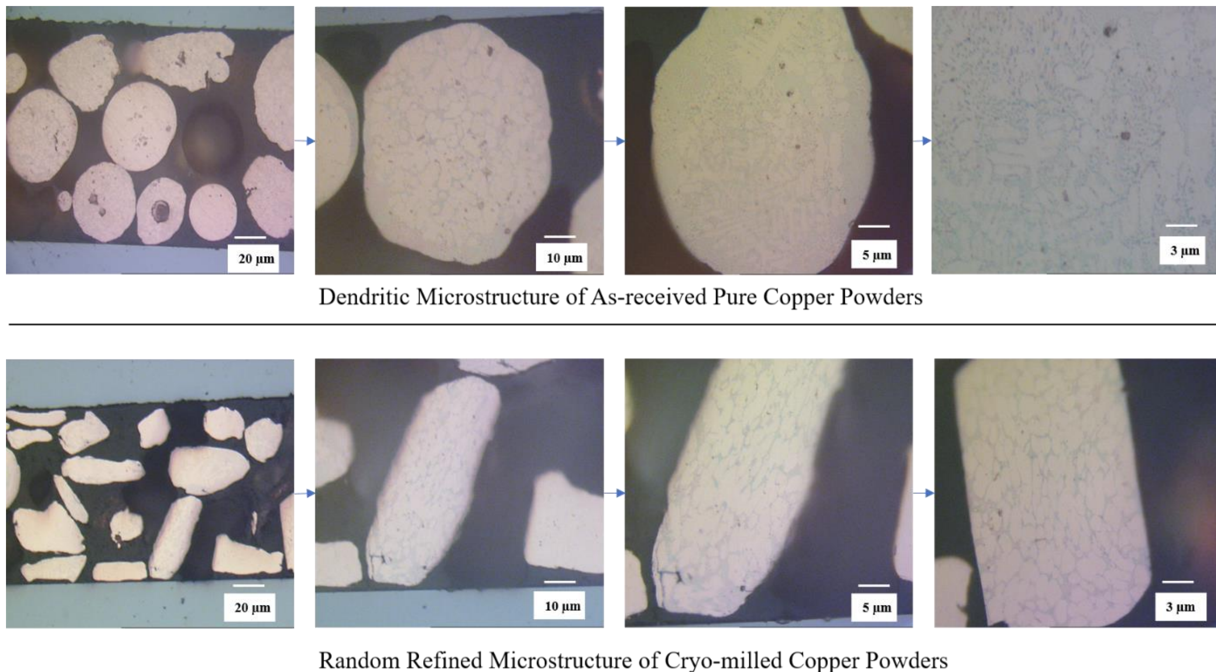

Figure 5. Optical Microscopy images of pure as-received pure Cu powders (**top** images) and cryo-milled Cu powders (**bottom** images) revealing inherent microstructures.

Furthermore, the EBSD analysis was conducted on the as-received pure Cu and cryo-milled Cu to observe their crystallographic texture, grain sizes, and grain boundary misorientation angles (Figure 6). The inverse pole figure (IPF) of pure Cu powders shows coarser grains that are uniformly orientated throughout the particle and have low grain boundary misorientation angles, as presented in Figure 6a. On the contrary, the cryo-milled Cu powders possess finer grains with highly random orientations and various size distributions, as shown in Figure 6b. The grain size distributions with their area fractions

are shown in Figure 6c. The grain sizes of the as-received pure Cu with substantial area fractions were found to be distributed mostly within the range of 1 µm to 5 µm, with an average size of around 3 µm; the grain sizes of the cryo-milled Cu with significant area fractions were within the range of 200 nm to 2 µm, and the average grain size was around 500 nm. Thus, the cryo-milling process was able to transform the coarse-grained (CG) powder particles into both fine-grain (FG) and ultrafine grained (UFG) powders. This grain refinement is crucial in activating the grain boundary strengthening mechanism in the subsequently consolidated bulk materials [10], which is the objective of this project.

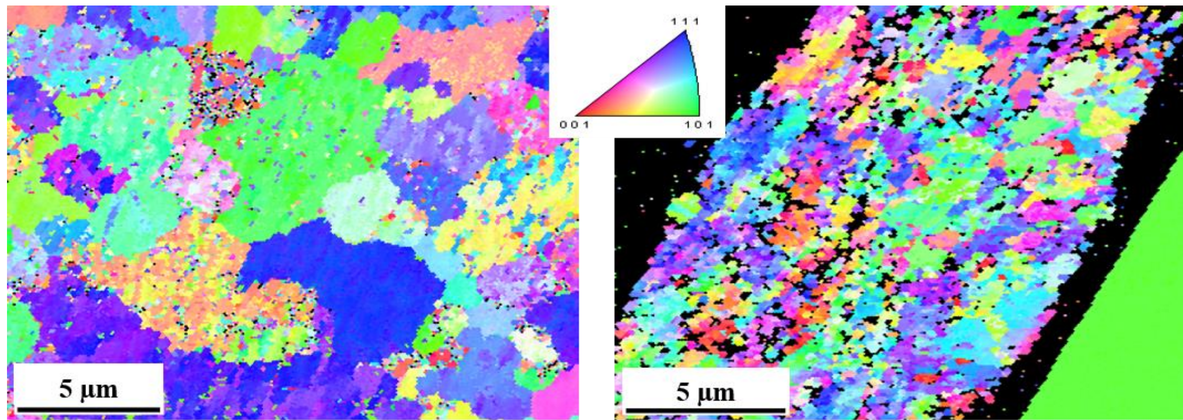

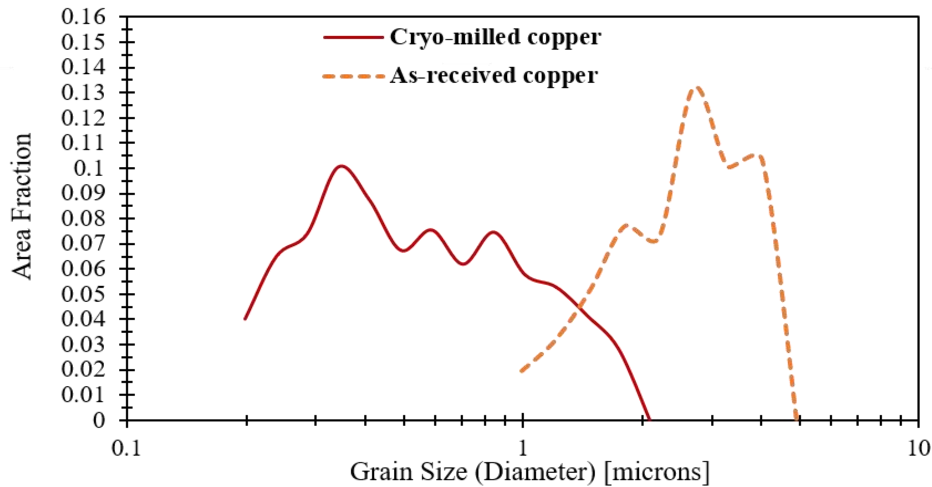

Figure 6. EBSD inverse pole figure (IPF) maps of the (**a**) as-received Cu and (**b**) cryo-milled Cu showing grain size orientation and distribution along with the color-coded map of IPF. (**c**) Grain size distribution of the as-received Cu and cryo-milled Cu.

The grain boundary misorientation angle distribution with their number fraction was analyzed for both the as-received Cu and cryo-milled Cu, as shown in Figure 7. The as-received pure Cu had mostly low angle grain boundaries within the range of 2.6 degrees to 9 degrees, with an average of 5.8 degrees. In contrast, the cryo-milled Cu grain has a mixture of low angle and high angle grain boundaries distributed between 2.6 degrees to 60.2 degrees, with an average of around 14.72 degrees. The average grain boundary misorientation angle of pure Cu increased more than two times after the cryo-milling process. These finer grains are developed from the coarser grains during cryo-milling because of the formation of sub-grain structures from the shear bands generated from the localization of the dislocations [43].

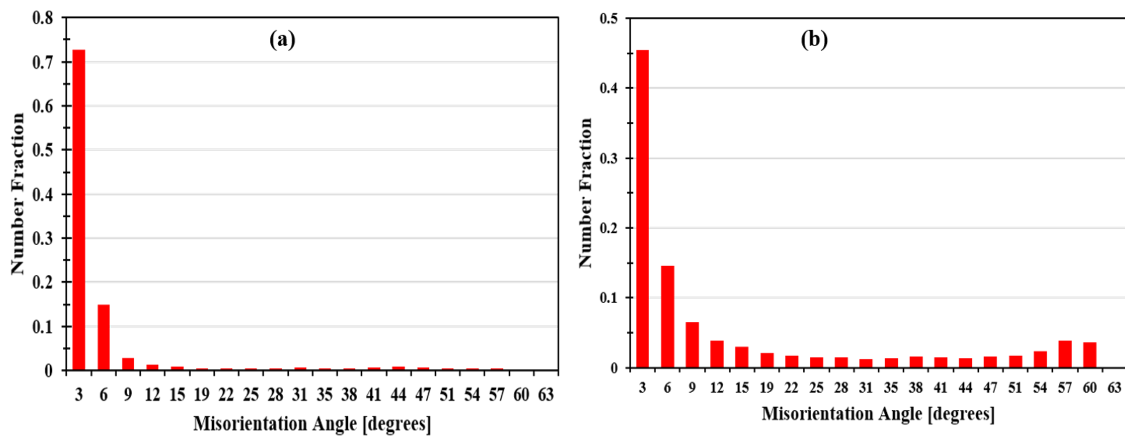

Figure 7. Grain boundary misorientation angle distribution of the (**a**) as-received Cu and (**b**) cryo-milled Cu.

3.3. Cold Isostatic Pressing of Cryo-Milled Powders

Though the cryo-milled powders showed excellent consolidation at 303 MPa pressure with good shape and sufficient green strength for handling, the as-received pure powders failed to consolidate properly, as shown in Figure 8. At pressures lower than 303 MPa, the cryo-milled powder did not consolidate well, as seen in Figure 8b. At 303 MPa the consolidation was excellent, as presented in Figure 8c.

Figure 8. Consolidated CIPed bars, (**a**) as-received pure Cu at 303 MPa, (**b**) cryo-milled Cu at 207 MPa, and (**c**) cryo-milled Cu at 303 MPa.

The 3D X-ray Computer Tomography (CT) scan of the CIPed sample was used to measure the internal porosity of the cryo-milled bulk Cu sample CIPed at 303 MPa, as shown in Figure 9. The black areas in the figures are porosity, which was measured to be ~48% of the volume of the sample.

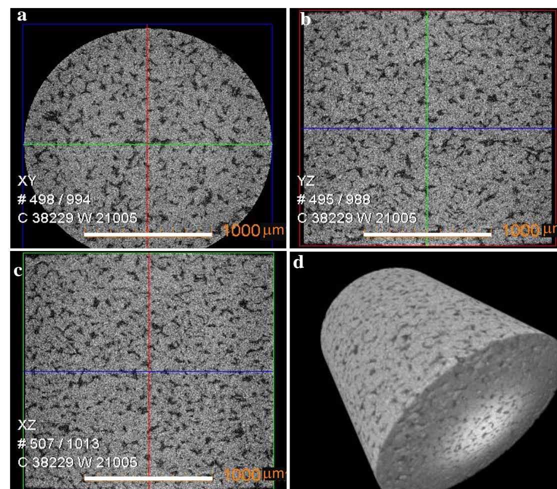

Figure 9. D X-ray tomography of cryo-milled Cu powder consolidated using cold isostatic pressing (**a**) 2D image from XY direction, (**b**) 2D image from YZ direction, (**c**) 2D image from XZ direction, and (**d**) 3D image of the sample. Scale bar in (**a**–**c**) is 1000 µm.

3.4. C-ECAP Processing of CIPed Cu Sample

Various severe plastic deformation (SPD) methods such as equal-channel angular pressing (ECAP), high-pressure torsion (HPT), multi-axial compression, accumulative roll bonding, and multi-directional roll bonding are available to improve the strength and ductility of different materials [10,15,31,32,44–50]. The ECAP can impart extremely large magnitudes of strain through shear, and thereby can produce nonporous billets by processing large bulk rods. The ECAP is highly capable of producing ultrafine-grained (UFG) and nanostructured (NS) materials from coarse-grained (CG) materials. During the ECAP of UFG materials, the gradual conversion of incidental dislocation boundaries (IDBs) into high angle grain boundaries (HAGBs) normally occurs, which in turn can contribute to grain boundary (GB) strengthening. Therefore, the material strengthening during ECAP is a result of both the dislocation strengthening in accordance with Taylor relation [51] and the grain boundary strengthening according to the Hall–Petch relation [51]. Moreover, the increment in HAGBs can contribute to GB sliding mechanism activation during material deformation, resulting in enhanced ductility [10,15,46]. In a study conducted by Alawadhi et al. [50], pure Cu exhibited considerable grain refinement following several ECAP passes. They have demonstrated that an initial average grain size of ~24 µm of oxygen-free pure Cu has reduced to ~16 µm, ~4.4 µm, and ~2.9 µm, respectively, after the one, four, and eight passes of ECAP at the 298 K temperature. Additionally, they observed that the orientation of the grains changed considerably towards equiaxed grains after higher ECAP passes. The low-angle grain boundaries (LAGBs) having misorientation angles between 2° and 15° transformed to high-angle grain boundaries (HAGBs) with misorientation angles greater than 15 ° following a higher number of ECAP passes. The fraction of HAGBs increased to ~71% after eight passes, as compared to ~25% after one ECAP pass. Moreover, the high number of ECAP passes showed that it can result in higher dislocation density along with lower crystallite size compared to the sample with fewer ECAP passes [50]. Again, the die angles and the number of passes dictate the equivalent plastic strain that is applied to the ECAPed sample.

Solid Cu rods CIPed at 303 MPa with 12–16 mm diameter went through continuous C-ECAP (C-ECAP) processing.

C-ECAP processing of the samples described above was completed using the C-ECAP machine operated by the Transdisciplinary Nanostructured Materials Research Team (TNMRT). For all processing, the machine was set-up using the tooling with a 12 mm die channel and 120° shear die. The processing parameters for all samples and each pass can be found below in Table 3.

Table 3. C-ECAP Processing Conditions.

	Pass 1	Pass 2	Pass 3	Pass 4
Feed rate (mm/sec)	6.3	6.3	6.3	6.3
ECAP Temp (°C)	130	130	140	140
Exit Channel Gap	11.79	11.65	11.85	11.71
Lubrication	None	None	None	None

Prior to being fed into the heated C-ECAP Machine on each pass, samples were soaked in a tube furnace adjacent to the machine for 10 min at 125 °C. Processing varied somewhat between passes because the technique and parameters resulted in partial bonding of the aluminum inter-sample rod used to separate each sample from the next sample. Bonded rods had to be separated from each other so that they could be fed back into the C-ECAP machine for subsequent passes. The final samples are shown in Figure 10.

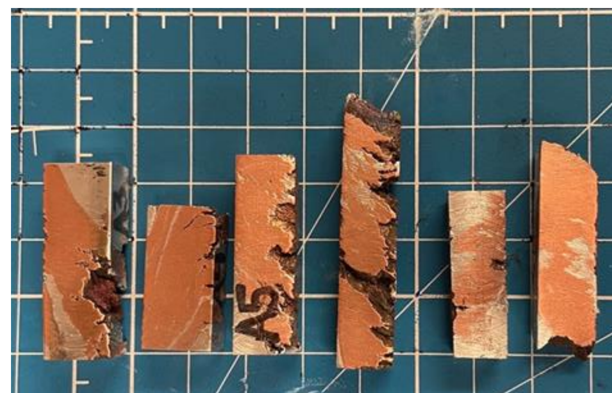

Figure 10. Samples following the C-ECAP Process.

3.5. Characterization of C-ECAPed Sample

The CIPed Cu bar with UFG and FG microstructure was further refined through the C-ECAP processing. Figure 11a,b show the low and high magnification optical microscopy of the cryo-milled Cu after CIP followed by C-ECAP processes, respectively. Nanoscale grain structures were achieved with excellent homogenous equiaxed grain orientations. The grain boundaries are visible in the figure, and it can be observed that the grain sizes reached below 100 nm after C-ECAP. Therefore, the following steps were used to fabricate a nanostructured Cu: (1) cryo-milling of powder, (2) CIP of cryo-milled powder, and (3) C-ECAP of the CIPed sample.

The C-ECAPed Cu sample exhibited electrical conductivity of ~74% ± 3.9 IACS at a measurement frequency of 60 kHz. This value is in the range of reported Cu metal currently used in railguns [17].

Hardness and elastic modulus were measured in continuous stiffness measurement (CSM) mode as a function of depth from zero to 3000 nm in displacement control mode, as shown in Figure 12. Figure 12a shows the load-displacement plots, and hardness and modulus versus displacement are shown in Figure 12b,c, respectively. The hardness and modulus were averaged in the depth range of 1000–3000 nm, where hardness is independent of depth. The C-ECAPed Cu sample showed a hardness of 163 ± 12.24 HV and a modulus of 134.16 ± 7.7 GPa.

Zhang et al. provided a general relationship that can be used to calculate the yield strength and ultimate tensile strength using nanoindentation results [52]. The yield strength and ultimate tensile strength of the C-ECAPed sample were found to be considerably superior to the traditional coarse-grained Cu bar, as presented in Table 4. There was a 158% increase in Vickers hardness value after the C-ECAP processing of the cryo-milled Cu

sample compared to the coarse-grained Cu. The elastic modulus is also 15% higher in the former case. Similarly, the ultimate tensile strength of the refined Cu was almost two times greater than the latter.

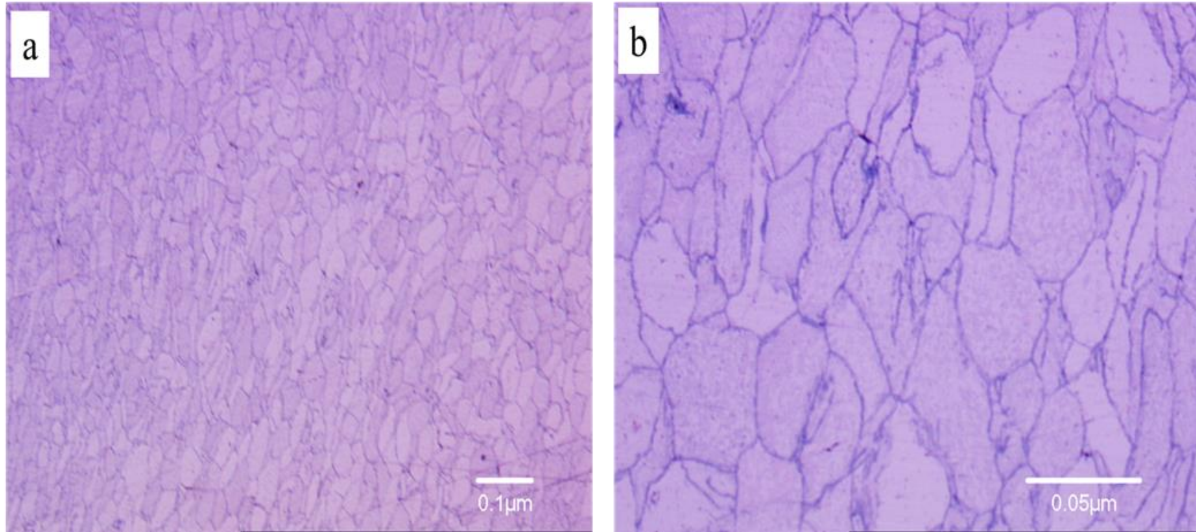

Figure 11. Optical microscopy of cryo-milled Cu powder after CIP followed by C-ECAP (**a**) low magnification and (**b**) high magnification.

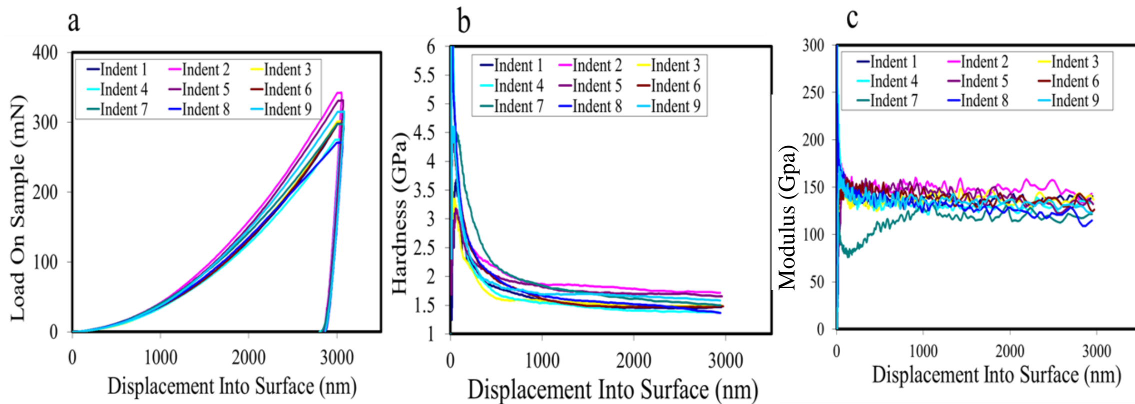

Figure 12. Nano-hardness measurement of C-ECAPed sample (**a**) load-displacement, (**b**) hardness versus displacement, and (**c**) modulus as a function of displacement. Nine indents were performed to ensure repeatability of the data.

The yield strength and the ultimate tensile strength of C-ECAPed Cu are very close, which is an indication of almost perfect plastic behavior.

Table 4. Summary of properties achieved for processed Cu with substantial grain refinement compared to the coarse-grained Cu.

Materials	Grain Size (µm)	Hardness (HV)	Elastic Modulus (GPa)	Yield Strength (MPa)	Ultimate Tensile Strength (MPa)	Electrical Conductivity (%IACS)
Coarse-grained Cu [53,54]	>50	63	117	79	241	101
Refined Cu in this analysis	<0.1	163	134.16	462	470	74

In summary the bi-modal grain size structure that was achieved showed great mechanical and electrical properties. Cu with this type of microstructure will have many functional applications including lighting shields [55] for aerospace, electrical conductors for railgun applications, and even uses in energy storage applications [56].

4. Conclusions

In conclusion, a combination of fine and ultrafine grains was obtained for Cu powder after cryo-milling at optimum conditions. The powder particles underwent continuous flattening, cold welding, and eventual fracturing into finer particles. The initial flattening and cold-welding resulted in a localization of deformation and subsequently decreased the grain size to the nanoscale. Further processing through cold isostatic pressing at an ambient temperature and 303 MPa did not change the microstructure significantly. Instead, porous Cu rods with good shape and sufficient green strength were created after the CIP process. Further consolidation was needed to obtain non-porous Cu billets. Therefore, these Cu rods went through continuous-ECAP processing. During C-ECAP, UFG and FG microstructures of the Cu became nanostructured and formed homogenous microstructures with grain sizes below 100 nm. These refinement procedures are believed to provide both increased strength and ductility to the materials. The hardness and modulus of the samples were ~1.6 GPa and ~134 GPa, respectively. The C-ECAP bulk Cu sample showed electrical conductivity of ~74% IACS, which was comparable to the Cu alloys currently used in railguns. Furthermore, the tensile strength of the C-ECAPed sample was around two times higher than the coarse-grained pure Cu.

Author Contributions: Conceptualization, methodology, investigation, original draft preparation, funding acquisition, project supervision and administration, L.L., Methodology, analysis of the results and C-ECAP addition, T.C.L., resources, data acquisition, data curation, review and editing, funding acquisition, J.R. All authors have read and agreed to the published version of the manuscript.

Funding: This research was funded by ONR under grant number: N00014-20-1-2436.

Data Availability Statement: Data is not publicly available.

Acknowledgments: We cordially acknowledge the financial support received during this project from the Office of Naval Research (ONR) under grant number: N00014-20-1-2436. We also acknowledge the technical support from Mark Thomason from Gasbarre Products Inc. and Kevin Miles and Bradley Harger from the Transdisciplinary Nanostructured Materials Research Team at the Colorado School of Mines.

Conflicts of Interest: The authors declare no conflict of interest.

References

1. Callister, W.D., Jr.; Rethwisch, D.G. *Materials Science and Engineering: An Introduction*, 10th ed.; Wiley: Hoboken, NJ, USA, 2020.
2. Hall, E.O. The deformation and ageing of mild steel: III Discussion of results. *Proc. Phys. Soc. Sect. B* **1951**, *64*, 747–753. [CrossRef]
3. Petch, N.J. The Cleavage Strength of Polycrystals. *J. Iron Steel Inst.* **1953**, *174*, 25–28.
4. Chokshi, A.; Rosen, A.; Karch, J.; Gleiter, H. On the Validity of the Hall—Petch Relationship In Nanocrystalline Materials. *Scr. Met.* **1989**, *23*, 1679–1683. [CrossRef]
5. Magee, A.C.; Ladani, L. Deformation and Failure of an Al-Mg Alloy Investigated Through Multiscale Microstructural Models. In *Light Metals*; Springer: Cham, Switzerland, 2015; pp. 245–249.
6. Magee, A.C.; Ladani, L.J. Temperature Effects in Al 5083 with a Bimodal Grain Size. *MRS Proc.* **2013**, *1513*, 5. [CrossRef]
7. Magee, A.C.; Ladani, L. Representation of a microstructure with bimodal grain size distribution through crystal plasticity and cohesive interface modeling. *Mech. Mater.* **2015**, *82*, 1–12. [CrossRef]
8. Nelson, S.; Ladani, L.; Topping, T.; Lavernia, E. Fatigue and monotonic loading crack nucleation and propagation in bimodal grain size aluminum alloy. *Acta Mater.* **2011**, *59*, 3550–3570. [CrossRef]
9. Ladani, L.; Nelson, S. Transition of crack propagation path under varied levels of load in bimodal grain size Al-Mg alloy. *J. Eng. Mater. Technol.* **2011**, *133*, 7–12. [CrossRef]
10. Morozova, A.; Kaibyshev, R. Grain refinement and strengthening of a Cu–0.1Cr–0.06Zr alloy subjected to equal channel angular pressing. *Philos. Mag.* **2017**, *97*, 2053–2076. [CrossRef]
11. Wen, H.; Topping, T.D.; Isheim, D.; Seidman, D.N.; Lavernia, E.J. Strengthening mechanisms in a high-strength bulk nanostructured Cu-Zn-Al alloy processed via cryomilling and spark plasma sintering. *Acta Mater.* **2013**, *61*, 2769–2782. [CrossRef]

12. Shangina, D.; Bochvar, N.; Morozova, A.; Belyakov, A.; Kaibyshev, R.; Dobatkin, S. Effect of chromium and zirconium content on structure, strength and electrical conductivity of Cu-Cr-Zr alloys after high pressure torsion. *Mater. Lett.* **2017**, *199*, 46–49. [CrossRef]
13. Dobatkin, S.; Gubicza, J.; Shangina, D.; Bochvar, N.; Tabachkova, N. High strength and good electrical conductivity in Cu-Cr alloys processed by severe plastic deformation. *Mater. Lett.* **2015**, *153*, 5–9. [CrossRef]
14. Wang, Y.; Fu, R.; Li, Y.; Zhao, L. A high strength and high electrical conductivity Cu-Cr-Zr alloy fabricated by cryogenic friction stir processing and subsequent annealing treatment. *Mater. Sci. Eng. A* **2019**, *755*, 166–169. [CrossRef]
15. Vinogradov, A.; Patlan, V.; Suzuki, Y.; Kitagawa, K.; Kopylov, V. Structure and properties of ultra-fine grain Cu-Cr-Zr alloy produced by equal-channel angular pressing. *Acta Mater.* **2002**, *50*, 1639–1651. [CrossRef]
16. Nayak, S.; Wollgarten, M.; Banhart, J.; Pabi, S.; Murty, B. Nanocomposites and an extremely hard nanocrystalline intermetallic of Al-Fe alloys prepared by mechanical alloying. *Mater. Sci. Eng. A* **2010**, *527*, 2370–2378. [CrossRef]
17. Xie, H.-B.; Yang, H.-Y.; Yu, J.; Gao, M.-Y.; Shou, J.-D.; Fang, Y.-T.; Liu, J.-B.; Wang, H.-T. Research progress on advanced rail materials for electromagnetic railgun technology. *Def. Technol.* **2020**, *17*, 429–439. [CrossRef]
18. Xu, C.; Wang, Q.; Zheng, M.; Zhu, J.; Li, J.; Huang, M.; Jia, Q.; Du, Z. Microstructure and properties of ultra-fine grain Cu-Cr alloy prepared by equal-channel angular pressing. *Mater. Sci. Eng. A* **2007**, *459*, 303–308. [CrossRef]
19. Islamgaliev, R.K.; Nesterov, K.M.; Bourgon, J.; Champion, Y.; Valiev, R.Z. Nanostructured Cu-Cr alloy with high strength and electrical conductivity. *J. Appl. Phys.* **2014**, *115*, 194301. [CrossRef]
20. Huang, J.Y.; Liao, X.Z.; Zhu, Y.T.; Zhou, F.; Lavernia, E.J. Grain boundary structure of nanocrystalline Cu processed by cryomilling. *Philos. Mag.* **2003**, *83*, 1407–1419. [CrossRef]
21. Attia, U.M. Cold-isostatic pressing of metal powders: A review of the technology and recent developments. *Crit. Rev. Solid State Mater. Sci.* **2021**, *46*, 587–610. [CrossRef]
22. Ka, U.B.; Panemangalore, D.B.; Bhat, S. Advanced Welding and Deforming: Equal channel angular processing-a modern deforming technique for quality products. In *Handbooks in Advanced Manufacturing*; Elsevier: Amsterdam, The Netherlands, 2021; Chapter 14; pp. 381–423. [CrossRef]
23. Murashkin, M.Y.; Sabirov, I.; Kazykhanov, V.U.; Bobruk, E.V.; Dubravina, A.A.; Valiev, R.Z. Enhanced mechanical properties and electrical conductivity in ultrafine-grained Al alloy processed via ECAP-PC. *J. Mater. Sci.* **2013**, *48*, 4501–4509. [CrossRef]
24. Shuai, G.; Li, Z.; Zhang, D.; Tong, Y.; Li, L. The mechanical property and electrical conductivity evolution of Al–Fe alloy between room temperature and elevated temperature ECAP. *Vacuum* **2020**, *183*, 109813. [CrossRef]
25. Magee, A. *Mechanical Properties and Microstructural Characteristics of an Al-Mg Alloy with Bimodal Grain Size at Room and Elevated Temperatures*; Institutional Repository, University of Alabama: Tuscaloosa, AL, USA, 2012.
26. Youssef, K.; Sakaliyska, M.; Bahmanpour, H.; Scattergood, R.; Koch, C. Effect of stacking fault energy on mechanical behavior of bulk nanocrystalline Cu and Cu alloys. *Acta Mater.* **2011**, *59*, 5758–5764. [CrossRef]
27. Langdon, T.G. Twenty-five years of ultrafine-grained materials: Achieving exceptional properties through grain refinement. *Acta Mater.* **2013**, *61*, 7035–7059. [CrossRef]
28. Sasaki, T.; Ohkubo, T.; Hono, K. Microstructure and mechanical properties of bulk nanocrystalline Al-Fe alloy processed by mechanical alloying and spark plasma sintering. *Acta Mater.* **2009**, *57*, 3529–3538. [CrossRef]
29. Botcharova, E.; Freudenberger, J.; Schultz, L. Mechanical and electrical properties of mechanically alloyed nanocrystalline Cu-Nb alloys. *Acta Mater.* **2006**, *54*, 3333–3341. [CrossRef]
30. Sabirov, I.; Murashkin, M.; Valiev, R. Nanostructured aluminium alloys produced by severe plastic deformation: New horizons in development. *Mater. Sci. Eng. A* **2013**, *560*, 1–24. [CrossRef]
31. Valiev, R.Z.; Langdon, T.G. Principles of equal-channel angular pressing as a processing tool for grain refinement. *Prog. Mater. Sci.* **2006**, *51*, 881–981. [CrossRef]
32. Wei, K.X.; Wei, W.; Wang, F.; Du, Q.B.; Alexandrov, I.V.; Hu, J. Microstructure, mechanical properties and electrical conductivity of industrial Cu-0.5%Cr alloy processed by severe plastic deformation. *Mater. Sci. Eng. A* **2011**, *528*, 1478–1484. [CrossRef]
33. Zhao, Y.; Topping, T.; Li, Y.; Lavernia, E.J. Strength and ductility of bi-modal Cu. *Adv. Eng. Mater.* **2011**, *13*, 865–871. [CrossRef]
34. Ma, K.; Wen, H.; Hu, T.; Topping, T.D.; Isheim, D.; Seidman, D.N.; Lavernia, E.J.; Schoenung, J.M. Mechanical behavior and strengthening mechanisms in ultrafine grain precipitation-strengthened aluminum alloy. *Acta Mater.* **2014**, *62*, 141–155. [CrossRef]
35. Milligan, J.; Vintila, R.; Brochu, M. Nanocrystalline eutectic Al-Si alloy produced by cryomilling. *Mater. Sci. Eng. A* **2009**, *508*, 43–49. [CrossRef]
36. Harrell, T.J.; Topping, T.D.; Wen, H.; Hu, T.; Schoenung, J.M.; Lavernia, E.J. Microstructure and Strengthening Mechanisms in an Ultrafine Grained Al-Mg-Sc Alloy Produced by Powder Metallurgy. *Met. Mater. Trans. A* **2014**, *45*, 6329–6343. [CrossRef]
37. Witkin, D.; Lavernia, E. Synthesis and mechanical behavior of nanostructured materials via cryomilling. *Prog. Mater. Sci.* **2006**, *51*, 1–60. [CrossRef]
38. Fecht, H.-J. Nanostructure formation by mechanical attrition. *Nanostructured Mater.* **1995**, *6*, 33–42. [CrossRef]
39. Bahmanpour, H.; Youssef, K.M.; Scattergood, R.O.; Koch, C.C. Mechanical behavior of bulk nanocrystalline copper alloys produced by high energy ball milling. *J. Mater. Sci.* **2011**, *46*, 6316–6322. [CrossRef]
40. Vogt, R.; Zhang, Z.; Topping, T.; Lavernia, E.; Schoenung, J. Cryomilled aluminum alloy and boron carbide nano-composite plate. *J. Mater. Process. Technol.* **2009**, *209*, 5046–5053. [CrossRef]

41. Maisano, A.J. *Cryomilling of Aluminum-Based and Magnesium-Based Metal Powders*; Virginia Polytechnic Institute and State University: Blacksburg, VA, USA, 2006.
42. Hanna, W.M. *Behavior and Microstructure in Cryomilled Aluminum alloy Containing Diamondoids Nanoparticles*; University of California Irvine: Irvine, CA, USA, 2013.
43. Ferrasse, S.; Hartwig, K.T.; Goforth, R.E.; Segal, V.M. Microstructure and properties of copper and aluminum alloy 3003 heavily worked by equal channel angular extrusion. *Met. Mater. Trans. A* **1997**, *28*, 1047–1057. [CrossRef]
44. Tao, X. *An EBSD Study on Mapping of Small Orientation Differences in Lattice Mismatched Heterostructures*; Lehigh University: Bethlehem, PA, USA, 2003.
45. Alihosseini, H.; Zaeem, M.A.; Dehghani, K.; Faraji, G. Producing high strength aluminum alloy by combination of equal channel angular pressing and bake hardening. *Mater. Lett.* **2015**, *140*, 196–199. [CrossRef]
46. Stoica, G.M. *Equal-Channel-Angular Processing (ECAP) of Materials: Experiment and Theory*; University of Tennessee: Knoxville, TN, USA, 2007.
47. Hockauf, M.; Meyer, L.; Zillmann, B.; Hietschold, M.; Schulze, S.; Krüger, L. Simultaneous improvement of strength and ductility of Al-Mg-Si alloys by combining equal-channel angular extrusion with subsequent high-temperature short-time aging. *Mater. Sci. Eng. A* **2009**, *503*, 167–171. [CrossRef]
48. Matsuki, K.; Aida, T.; Takeuchi, T.; Kusui, J.; Yokoe, K. Microstructural characteristics and superplastic-like behavior in aluminum powder alloy consolidated by equal-channel angular pressing. *Acta Mater.* **2000**, *48*, 2625–2632. [CrossRef]
49. Bongale, A.M.; Kumar, S. Equal channel angular pressing of powder processed Al6061/SiC nano metal matrix composites and study of its wear properties. *Mater. Res. Express* **2018**, *5*, 035002. [CrossRef]
50. Alawadhi, M.Y.; Sabbaghianrad, S.; Wang, Y.C.; Huang, Y.; Langdon, T.G. Characteristics of grain refinement in oxygen-free copper processed by equal-channel angular pressing and dynamic testing. *Mater. Sci. Eng. A* **2020**, *775*, 138985. [CrossRef]
51. Torre, F.H.D.; Gazder, A.A.; Gu, C.F.; Davies, C.H.; Pereloma, E.V. Grain size, misorientation, and texture evolution of copper processed by equal channel angular extrusion and the validity of the Hall-Petch relationship. *Met. Mater. Trans. A* **2007**, *38*, 1080–1095. [CrossRef]
52. Zhang, P.; Li, S.; Zhang, Z. General relationship between strength and hardness. *Mater. Sci. Eng. A* **2011**, *529*, 62–73. [CrossRef]
53. Wu, Y.; Huang, S.; Chen, Q.; Feng, B.; Shu, D.; Huang, Z. Microstructure and Mechanical Properties of Copper Billets Fabricated by the Repetitive Extrusion and Free Forging Process. *J. Mater. Eng. Perform.* **2019**, *28*, 2063–2070. [CrossRef]
54. Ellingsen, D.A.G.G.; Horn, N.; Aaseth, J.A.N. Copper. In *Handbook on the Toxicology of Metals*, 5th ed.; Academic Press: New York, NY, USA, 2007. [CrossRef]
55. Alemour, B.; Badran, O.; Hassan, M.R. A review of using conductive composite materials in solving lightening strike and ice accumulation problems in aviation. *J. Aerosp. Technol. Manag.* **2019**, *11*, 1–23. [CrossRef]
56. Shi, C.; Wang, T.; Liao, X.; Qie, B.; Yang, P.; Chen, M.; Wang, X.; Srinivasan, A.; Cheng, Q.; Ye, Q.; et al. Accordion-like stretchable Li-ion batteries with high energy density. *Energy Storage Mater.* **2018**, *17*, 136–142. [CrossRef]

Disclaimer/Publisher's Note: The statements, opinions and data contained in all publications are solely those of the individual author(s) and contributor(s) and not of MDPI and/or the editor(s). MDPI and/or the editor(s) disclaim responsibility for any injury to people or property resulting from any ideas, methods, instructions or products referred to in the content.